A micro-Particle Image Velocimetry approach to flow measurements in isolated contracting lymphatic vessels

K. N. Margaris,[a] Z. Nepiyushchikh,[b] D. C. Zawieja,[c] J. Moore, Jr.,[d] R. A. Black,[e]

[a]University of Strathclyde, Department of Biomedical Engineering, 106 Rottenrow, Glasgow, UK, G4 0NW, E-mail: kmargaris@gmail.com

[b]Georgia Institute of Technology, The George W. Woodruff School of Mechanical Engineering, Georgia Institute of Technology, Atlanta, Georgia, USA, 30332-0405, E-mail: zhanna.nepiyushchikh@me.gatech.edu

[c]Texas A&M University, Department of Systems Biology and Translational Medicine, Health Science Center, Temple, Texas, USA, 77843-111, E-mail: dcz@tamu.edu

[d]Imperial College, Department of Bioengineering, London, UK, SW7 2AZ, E-mail: james.moore.jr@imperial.ac.uk

[e]University of Strathclyde, Department of Biomedical Engineering, 106 Rottenrow, Glasgow, UK, G4 0NW, E-mail: richard.black@strath.ac.uk

Address all correspondence to: K. N. Margaris, University of Strathclyde, Department of Biomedical Engineering, 106 Rottenrow, Glasgow, UK, G4 0NW; E-mail: kmargaris@gmail.com

Abstract. We describe the development of an optical flow visualization method for resolving the flow velocity vector field in lymphatic vessels, *in vitro*. The aim is to develop an experimental protocol for accurately estimating flow parameters, such as flow rate and shear stresses, with high spatial and temporal resolution. Previous studies *in situ* have relied on lymphocytes as tracers, but their low density resulted in a reduced spatial resolution whereas the assumption that the flow was fully developed in order to determine the flow parameters of interest may not be valid, especially in the vicinity of the valves, where the flow is undoubtedly more complex. To overcome these issues, we have applied the time-resolved micro-Particle Image Velocimetry technique, a well-established method that can provide increased spatial and temporal resolution that this transient flow demands. To that end, we have developed a custom light source, utilizing high-power light-emitting diodes, and associated control and image processing software. This manuscript reports the performance of the system and the results of a series of preliminary experiments performed on vessels isolated from rat mesenteries, demonstrating, for the first time, the successful application of the micro-PIV technique in these vessels.

Keywords: Lymphatic system, lymphangion, micro-PIV, flow measurements, physiological flows, LED.

1 Introduction

The lymphatic system is a vital part of the circulatory and immune systems,[1,2] and plays an important role in tissue fluid homeostasis and in combating infection. In contrast with the cardiovascular system, where the heart provides the necessary energy for blood flow, the lymphatic system relies on the active contraction of individual vessels and one-way valves to generate and sustain flow. It consists of lymphatic capillaries, collecting lymphatic vessels and lymphoid organs. While the small lymphatic capillaries fill passively with interstitial fluid, the larger collecting lymphatic vessels actively contract to generate flow owing to local translumenal pressure and strain gradients within the extra-cellular matrix of the vessel wall. The ability of these vessels to contract originates from the smooth muscle cells (SMCs) that line the vessel wall, which are morphological similar and exhibit similar molecular signaling and pace-making abilities as cardiac SMCs.[3] Non-return, predominantly bicuspid, valves prevent the retrograde flow of lymphatic fluid. The portion of the vessel between two valves is referred to as a 'lymphangion'. Individual lymphangions are arranged in networks to form the lymphatic vessels.

Reported attempts to measure the flow field* inside these vessels are few in number. In fact, excluding studies on lymph filtration, the only study to quantify temporal variations of flow velocity during contraction was that conducted by Dixon and co-workers,[5–7] which was subsequently used in Kassis et al.[8] These studies were performed *in situ*, in the exteriorised rat mesenteric area. Lymphocytes were used as tracers and images were acquired with a high speed camera. An image correlation algorithm was used to measure the lymphocyte velocity.[9] The authors inferred the flow velocity, volumetric flow rate and wall shear stress by assuming that lymphocytes follow the flow

*The term 'flow field' used in the document refers to the flow velocity vector field in the mid-plane of a lymphatic vessel. A vector field is a collection of vectors of given direction and magnitude. Each vector is assigned to a given point in space.[4]

faithfully, and that the flow is laminar and fully developed. A major drawback of this approach is that the lymphocytes are relatively large in size (approximately 10 μm in diameter, whereas the vessel lumen diameter is on average 100 μm) and their density is usually low, reducing spatial resolution; hence the need to make assumptions with regard to the nature of the flow. Using lymphocytes as tracers limits the applicability to *in situ* measurements, and while such experiments may yield more physiologically relevant results with respect to an isolated *in-vitro* preparation, the use of latter allows more control over factors that affect lymphatic function. Moreover, the latter study employed continuous wave (CW) illumination, which can significantly reduce the temporal resolution of an optical flow measurement system, rendering such a system less capable of resolving transient changes to flow velocity that may occur during the vessel contraction cycle.

Despite these drawbacks, these studies have been the most recent and only attempts in estimating fluid velocity and its temporal variations inside collecting lymphatic vessels. Several other attempts have been made to measure lymphatic flow rate in a variety of species, however they are restricted to average flow rate measurements, tracking volumes of fluorescently tagged particles or fall under the flow cytometry methods; whilst very useful from a physiological or clinical perspective these methods cannot give a detailed description of the local fluidic environment and especially wall shear stresses which is an important parameter that affect lymphatic function.

Onizuka et al. and Naito et al. implanted an ultrasound flow probe in sheep to measure the flow rate of the thoracic duct.[10,11] The flow rates measured were three to six times greater than the ones measured in cannulated vessels and this fact was attributed to the invasive cannulation procedure. However, the authors did not clarify any effects the presence of the ultrasound probe had on the contraction of the thoracic duct. With this method there is no way to a priori exclude the possibility of the vessel coming into contact with the probe as it contracts. The authors did not

report measurements of lymph velocity or of wall shear stresses.

McGeown et al. used a method that utilizes a transducer to measure lymph flow rate in conscious sheep by means of vessel cannulation.[12] Lymph was let to accumulate on the transducer arm and the weight of the fluid caused a tension reading on the transducer. The reading of tension was correlated with lymph volume leaving the cannulated vessel. This method, however, does not yield detailed flow field information.

Fedosov et al. developed an invasive flow cytometry method using a focused laser beam.[13] The velocity and direction of lymphocytes was determined by cross-correlation of intensity fluctuations of the speckle field between two points. The method was applied *in vivo* in the rat mesenteric area, however very limited results on measurements from different vessels were presented. Whether the method is able to measure a 2-dimensional flow field is unclear from the work published. According to[13] the velocity measured is in relative units and therefore calibration was necessary with video microscopy. Using a focused laser beam also raises concern of potential damage of the lymphatic vessels.

Similarly to the work by Fedosov et al., Kalchenko et al. developed a label free *in vivo* laser speckle imaging for blod and lymph vessels.[14] Although the method is able to demarcate lymphatic vessels, the long correlation/exposure times of their method (200 ms) renders it unable to measure instantaneous flow velocity.

Galanzha et al. developed a photo-acoustic flow cytometry method to count normal and abnormal immune cells in[15] in collecting lymphatic vessels *in vivo* in the rat mesentery and mouse ear. Using such approach it is possible to measure the velocity of lymphocytes, however it suffers the same drawbacks as the work by Dixon et al., that is, lymphocytes due to their larger size are not ideal tracers and due to their low density no spatial flow velocity information can be extracted

experimentally.

The aforementioned studies target the flow in larger collecting lymphatic vessels. Swartz et al.[16] and Berk et al.[17] utilized fluorescent photo-bleaching to measure the flow in the lymphatic capillaries of the mouse tail. The method uses a fluorescent dye, instead of cells or particle tracers. Similarly, Fischer et al.[18] used fluorescein isothiocyanate-dextran dye to measure flow velocity in lymphatic capillaries of the human skin. Although it is possible to measure velocity with fluorescent dyes, the lack of individual tracers reduces the spatial resolution and no spatially resolved flow fields were reported by the authors. Additionally, diffusion of the fluorescent dye induces experimental errors in determination of the fluid velocity.[19]

Non invasive *in vivo* methods have also been utilized in lymph flow measurements in lymphatic collecting vessels.[20,21] Vessels and nodes up to 3 cm below the surface were visualized with the use of near-infrared imaging with indocyanine green (ICG) tracer. However, longer wavelengths have an adverse impact on the intensity of light emitted which necessitates the use of more sensitive sensors and reduces the spatial resolution. These studies in swine displayed the capability of the method to measure average velocity of tagged 'packets' of ICG but no spatially resolved information can be obtained rendering the method unsuitable for accurately resolving the flow field in lymphatic vessels. Other non invasive *in vivo* lymphangiography methods have been developed using an optical coherence tomography (OCT) approach or optical microangiography (OMAG), a variant of OCT.[22,23] OCT lymphangiography allows for label free demarcation of lymphatic vessels and flow visualization. No quantitative information on flow in lymphatics was reported in these studies.

Motivated by the lack in available flow measurement methods, and in an attempt to overcome some of the limitations of previous work, we have employed the micro-Particle Image Velocime-

try method, or μ-PIV.[24] PIV involves seeding the flow with tracer particles, and uses statistical methods to resolve the fluid velocity from consecutive images acquired at a given location. By increasing the tracer concentration, and reducing the particle diameter, the spatial resolution may be increased. Smaller particles, being less subject to the effects of gravity or inertia, exhibit excellent frequency response and settling times far in excess of the time scales of interest, with the result that they follow the flow more faithfully and provide a more accurate representation of the actual flow field. Moreover, by appropriate synchronization of light pulses and image acquisition, that is, the frame-straddling technique, the temporal resolution of such system can be significantly increased.[25]

With the above observations in mind, we have developed a low-cost light source, using high-power light-emitting diodes (LEDs) as well as associated synchronization software. The resulting images were processed with open-source code, which was extended to incorporate vessel wall tracking algorithms and image filters. The purpose of this manuscript is to describe the development of the experimental apparatus and to present preliminary analysis of data acquired in vitro from images of actual mesenteric lymphatic vessels and valves, thus demonstrating the applicability of μ-PIV in these vessels.

2 Material & Methods

2.1 LED light source development

The LED light source utilizes high-power white and monochromatic LEDs (CBT-90 white/green, PT-120 green and CBT-140 white, Luminus Devices, USA, www.luminus.com). The driving electronics are from the same manufacturer (DK-136M development kit) and are capable of driving the LEDs with current pulses of up to 36A. The pulse width time is adjustable from $2\,\mu s$ to several

milliseconds. The pulse separation time Δt_p is also controllable and can be as low as $10\,\mu s$. Power is provided by a 650W power supply (XP Power, Singapore). Control and synchronization of the source was implemented with LABView and a multifunction DAQ device (National Instruments, USA). A five-axes kinematic mount (EKSMA Optics, Lithuania) provided alignment of the LED with a quartz fiber-optic light guide which delivered the light to an inverted microscope (Nikon, Zeiss). In order to increase the light collection efficiency of the LED-fiber optic interface, several lens combinations were tested and the highest radiometric power output was obtained with an aspheric condenser lens with numerical aperture (NA) of 0.9.

The output of each LED was measured with a power meter (Thorlabs PM100A/S120VC) while a spectrometer (AVS-MC2000, Avantes BV, The Netherlands) was used to obtain the spectrum of the emitted light. The images were acquired with several high-speed cameras: a Photron SA-3 and MC-1 (Photron Inc, USA) were used during the development phase at Strathclyde University, whereas a Phantom V5.2 (Vision Research, USA) was used at Texas A&M University were the experiments in lymphatic vessels took place.

2.2 Micro-fluidic experimental setup

2.2.1 Micro-PIV setup

A μ-PIV setup was constructed around a Zeiss inverted microscope (20x magnification), following the guidelines available in the literature.[19,24,26] The most significant difference with respect to a typical system (shown in Figure 1a) is the means of illumination, which is explained in detail below. The flow was seeded with micro-particles and the LED light source used provided suitable short burst pulses to capture the particle motion whilst minimizing streaking. Images were acquired by a CMOS camera (Vision Research, Phantom V5.2) and transferred to a computer for

analysis. The field of view of the CMOS sensor was $659x512$ μm, which was sufficient to focus on a middle section or a valve, but not large enough to fit two adjacent lymphangions. Although the sensor field of view (FOV) was smaller than the microscope objective FOV, the latter was not great enough to fit into view two adjacent lymphangions.

Pressure was adjusted by changing the height of the inflow and outflow reservoirs. Axial pressure gradient in this context is defined as $\Delta P_{axial} = P_{out} - P_{in}$. Therefore, when the inflow reservoir is raised higher than the outflow one, the pressure gradient is negative (favorable gradient) and drives the flow. In contrast, when the outflow reservoir is raised higher than the inflow one, ΔP_{axial} becomes positive (adverse gradient); forward flow, that is, flow along the direction of the vessel as allowed by the orientation of the one-way valves, cannot be maintained by the axial pressure gradient. The translumenal pressure P_{tr} is the average value of the inflow and outflow pressures minus the external hydrostatic pressure exerted by the fluid column above the vessel ($2\ cmH_2O$).

Non-fluorescent 1 μm particles (density $\rho = 1.05 g/cm^3$) were used. The particle response time is a function of the particle diameter d_p, particle density ρ_p and the fluid viscosity mu and is given in Equation 1. This time, in water at 37^o, is approximately $0.08\ \mu s$ is considered to be low enough for the flows under investigation in this study.[26] Their settling time is also long: it would take approximately 30 minutes for particles of 1 μm diameter to settle 50 μm, which is approximately the radius of rat mesenteric lymphatic vessels.[27] This time is long enough compared to the time scales of the flow in question so that the effects of gravity may be safely ignored for the flows under investigation.

(a) (b)

Fig 1: Experimental setup & Camera-Light synchronization.: (a) Typical μ-PIV setup. A light source illuminates particles seeded in the flow, with high frequency, short duration pulses, through a microscope objective. A camera captures images in synchrony with the light source which are transferred to a computer for spatial cross-correlation analysis. Although fluorescent particles are commonly used in μ-PIV, in the current setup non-fluorescent particles were used with the light been delivered from above and at an angle with respect to the specimen. Pressure was adjusted by changing the height of the inflow and outflow reservoirs. Image adapted with permission from Wereley and Meinhart.[30] (b) Injection port that was used to deliver particles. A 3-way valve was used to isolate the vessel during particle injection for protection against pressure.

$$\tau_p = d_p^2 \frac{\rho_p}{18\mu} \tag{1}$$

The particle diameter on the camera sensor (particle image diameter) is important and influences the random error in determining the particle displacement between frames.[19,26] The optimum particle image diameter that minimizes the random error corresponds to 2-4 pixels. With the current setup the particle image diameter was 3.9 pixels, as estimated by the following equation:[28]

$$d_\tau = \sqrt{(M \cdot d_p)^2 + (2.44 \cdot f_\#(M+1)\lambda)^2} \tag{2}$$

where, M is the microscope magnification, $f_\# = 1/(2NA)$ is the f-number, $NA = 0.5$ the numerical aperture of the objective, λ the wavelength of the light and d_p the physical particle diameter. This equation is in good agreement with experimental results at 20x magnification.[29]

Frame straddling is a method for increasing the temporal resolution of a PIV system and is illustrated in Figure 2. The light pulses are placed in such manner as to 'straddle' the inter-frame time, which defines the limit of the temporal resolution. In our system this time was $2\ \mu$s hence it was possible to have sufficient temporal resolution without increasing the frame rate of the camera;

it also reduces the image memory storage requirements[†]. The PIV pair of frames are acquired at half the camera frame rate, but modern cameras usually have high enough frame rate to compensate for the loss in acquisition rate. The camera frame rate was set to 10-500 fps and the pulse separation time adjusted so that the particle displacement was 5-10 pixels between frames. This is less than one quarter of a 64 pixels interrogation window and is considered to be a good choice in PIV experiments and often termed as the one-quarter rule (cf. Section 2.3). Since the expected flow velocity was not known it was necessary to take successive measurement with varying pulse separation time. Pulse separation time ranged from $10\,\mu s$ for flow at high negative pressure gradient, up to $10\,ms$ for flows at positive pressure gradient. The use of light pulses instead of continuous wave illumination has additional advantages: it reduces the amount of light that the vessels are exposed to and reduces the cooling requirements of the LEDs.

A typical microscopic view of a single lymphatic vessel under two forms of illumination is presented in Figure 3. When illuminated in bright-field mode via the epi-fluorescence module of the microscope (Fig. 3a), diffuse light scattered from the structures in and out of the focal plane is captured, reducing the effective contrast of the images. When illuminated from above (and at an angle) via the fiber-optic cable (Fig. 11a), however, the contrast of the images improves, with much of the light scattered from objects located within the focal plane of the microscope (Fig. 3b).

[†]In contrast, if frame-straddling is not used, the light source can be synchronized to provide one pulse per camera exposure at the center of each frame. However, this constrains the temporal resolution to the camera frame rate. In other words, setting the camera at 250 fps the temporal resolution becomes $1/250 = 4\ ms$ and to achieve a 2 μs resolution the camera needs to be set at 500,000 fps. Using continuous wave illumination has the same drawback too and in addition particle streaking may occur. Our research showed that even at adverse pressure gradients in lymphatics the required temporal resolution can be as low as 1 ms (1000 fps) hence the current implementation is capable of achieving this resolution without expending too much memory.

Fig 2: Example of frame straddling (F-S). The camera is set to record at a specific frame rate. In order to acquire one pair of images for PIV, the first light pulse is placed towards the end of the first frame (Frame 1A) and the second light pulse at the beginning of the second frame (Frame 1B) as to 'straddle' the inter-frame time. With this approach the time between frames is limited by the camera inter-frame time, or 2 μs in the current implementation. The next pair of frames (Frames 2A/2B) must be acquired at half the camera fps in order to avoid double exposure.

(a) (b)

Fig 3: Image of a lymphatic vessel and valve at 20x magnification: (a) bright-field and (b) side-scattering illumination mode. Here, light was delivered from a fibre-optic cable positioned above and at an angle of about 45 degrees with respect to the microscope stage. The low numerical aperture of the objective used (M = 20x, NA = 0.5) ensured that stray light from the bottom wall was not significant.

2.2.2 Isolated lymphatic vessel preparation protocol

All experiments involving ex-vivo lymphatic vessel preparations were carried out at the Texas A&M Health Science Center, Temple, Texas, USA. The animal facilities used for these studies were accredited by the Association for the Assessment and Accreditation of Laboratory Animal Care, and adhered to the regulations, policies, and principles detailed in the Public Health Service Policy for the Humane Care and Use of Laboratory Animals (PHS Policy, 1996) and the U.S. Department of Agricultures Animal Welfare Regulations (Animal Welfare Act, AWA, 9CFR, 1985, 1992). All animal procedures performed for this study were reviewed and approved by the Texas A&M Institutional Animal Care and Use Committee.

Mesenteric lymphatic vessels and segments of the thoracic duct were isolated from anesthetized Sprague-Dawley rats and cannulated in a vessel chamber. The bath solution was an albumin enriched physiological solution (APSS). The same liquid medium was used as solvent for the particle suspension. Details regarding the vessel isolation protocol can be found in Gashev et al.[31]

Polystyrene micro-particles of 1 μm diameter (Polysciences Europe GmbH, Germany) were either introduced into the upstream pipette with the vessel uncannulated to avoid damage, or via an injection port (Figure 1b). In the latter case the vessel was cannulated and was isolated by a 3-way valve to avoid damage during particle injection. Approximately 0.5ml of particle solution was required; after initial trials 0.5% weight-to-volume particle concentration was used in order to have 7-10 particles per interrogation window, which is an optimum value in PIV.[19] Data on the refractive index of lymphatic tissue are difficult to find in the literature. Galanzha et al.[32] report a value of 1.38 for rat mesenteric tissue, which is close to the refractive index of water (RI = 1.33). Therefore the major source of refractive index mismatch errors are likely to originate from the aperture on the vessel chamber bottom (RI = 1.58) and the air objective used (RI = 1). Temperature was regulated at physiological levels $36 - 38^oC$.

2.3 Image analysis

The image acquisition sequence generates a series of image pairs. Since the frame rate and pulse separation time are known, each pair of images may be spatially cross-correlated in order to calculate the velocity vectors of individual particles within the FOV. Briefly, a pair of frames is analyzed in each step. The images are divided into smaller interrogation windows (32x32 and 64x64 pixels in the present study). The interrogation windows from the two frames are cross-correlated and the resulting particle displacement divided by the pulse separation time to give the velocity vector associated with those particles within the interrogation window. Other flow parameters may be derived from the flow velocity field. More information on PIV cross-correlation algorithms can be found in the literature.[19,26]

Here the analysis was performed with the open-source Matlab toolbox PIVlab (version 1.32).[33]

Established image-processing macros for background subtraction and image enhancements were implemented,[34–36] and image overlapping algorithms were employed to compensate for low seeding density in the case of steady flows.[37] The filter that yielded the optimum results, in terms of noise reduction, was that developed by Gui and Wereley.[34] Figure 4 shows an image of a lymphatic vessels containing particles that has been processed with this filter.

In PIV, post-processing of the resulting vector field is necessary, in order to remove outliers from the results. PIVlab implements a number of post-processing options that are common in PIV analysis. Here, a novel automatic and robust method developed by Garcia[38] was used. This method is a penalized least square approach that allows for automatic smoothing of data in one or higher dimensions. Smoothing is carried out by direct cosine transformation. The degree of smoothing is determined by a minimization algorithm. The algorithm also deals efficiently with outliers or missing data. Further details can be found in the original publications.[38,39]

Vessel contraction adds an additional complexity to the problem: that of detecting the vessel wall in order to create a mask and remove the wall during cross-correlation[‡]. While manual masking is possible, it hinders the analysis of large data sets. A vessel wall detection algorithm was developed (Fig. 5 shows a representative result), based on Canny edge detection.[40] Prior to applying the Canny Edge detection, the images were pre-processed, by means of either thresholding or the application of mask filters.[41]

Fig 4: Image processed by a combination of unsharp and smoothing filters prior to PIV analysis.

Fig 5: Example of vessel wall detection. The red line denotes the detected vessel wall edge using Canny edge detection.

[‡]In some cases the vessel may also rotate or move perpendicular to the image plane during contraction. However, this can be avoided with careful vessel cannulation and ligation.

2.4 Wall shear stress estimation

The wall shear stress (WSS) was estimated by a curve-fitting procedure whereby a third order polynomial was fitted to the four velocity vectors derived from interrogation windows adjacent to the vessel wall. The wall shear stresses at a given axial location was taken to be the average of the values determined at opposite walls, in order to account for asymmetry in the velocity profile[§].

Since the experiments were carried out at physiological temperatures of $36 - 38^oC$ and APSS is an aqueous solution it was considered reasonable to assume that that APSS has the same properties as pure water at the same temperatures (density $\rho = 993\ kg/m^3$, dynamic viscosity $\mu = 6.78 \times 10^{-4}\ Pa \cdot s$).

3 Results

3.1 LED light source

The LED light source was characterized in terms of LED power output pulsed mode illumination (PM) at different levels of input current, pulse frequency and duty cycles. Figure 6 compares the energy per pulse of different LEDs from the same manufacturer, measured at a frequency of $1\ kHz$ with $100\ \mu$s pulse duration[¶]. During experiments in lymphatic vessels our system could yield good contrast with $50\ \mu$s pulse duration, hence the power per pulse was half the one reported in Figure 6.

The driver circuit can pulse the LED at frequencies of up to $3\ kHz$, with up to $36\ A$ current pulses. The time interval between two successive pulses can be as short as 5μs, which, taking

[§]In this implementation, the velocity from the PIV analysis at the wall was used; this is generally non-zero and although this deviates from the no-slip velocity condition at the wall it has been shown to yield more accurate results than replacing the velocity value at the wall with zero[42]

[¶]Generally, the optical power output required for such experiments is not reported in the literature, hence we show the indicative measurement in Figure 6, which may be of use to researchers planning similar experiments

into account the one-quarter rule in PIV,[43] corresponds to velocities in excess of 100 mm/s at 20x magnification.[44] While the mean flow velocity throughout the lymphatic system is generally lower than this value (under positive or zero pressure gradient the maximum velocity we observed was approximately 10 mm/s), under negative pressure gradient of $-5\ cmH_2O$ it can reach 50 mm/s (unpublished observations).

Fig 6: Power output of two white LEDs by Luminus Devices, CBT-90 and CBT-140. The measurement was performed at the exit of a 6 ft fiber-optic light guide. Despite the considerable losses at the LED/fiber-optic bundle interface, the power output is sufficient for optical flow diagnostic methods, such as the one presented here.

3.2 Micro-PIV system performance

In terms of spatial resolution, using 64 px interrogation windows (IW) with 75% overlap yields approximately 20 velocity vectors along the diameter of a fully distended vessel. This number is reduced to approximately 10 vectors at the end systolic diameter (ESD).

A detailed a priori analysis of the measurement uncertainty in PIV is generally not possible. Therefore, an a posteriori analysis has to be performed instead. The analysis which included the effects of the optical setup, random errors due to the PIV algorithm and Brownian motion, showed that the cumulative, measurement uncertainty, estimated at the maximum velocity at the center of the vessels, remained below 6% over the entire range of experiments performed (unpublished data).

The minimum resolvable velocity is given by the root mean square error in estimating the particle displacement between frames and may be estimated by the following equation:[45]

$$\sigma_u = \frac{c_\tau d_\tau}{M \Delta t} \tag{3}$$

For the current system the particle image diameter was d_τ was equivalent to 3.9 pixels at $M = 20x$ magnification. The constant c_τ is equal 1-10%. Assuming that $c_\tau = 5\%$ and Δt ranging from $10\ ms$ to $50\ \mu s$ the resulting minimum resolvable velocity is $0.56 - 111.74\ \mu m/s$ (the calibration factor for the system was $0.573\ \mu m$ per pixel).

As one would expected, the greater the favorable pressure gradient the greater is the corresponding flow velocity. It follows that the temporal resolution need not be so great to resolve the flow velocity, as is apparent in Figure 7. The relatively large deviation of data from the mean at each value of axial pressure gradient is due to the natural variation of vessel diameter from lymphangion to lymphangion of the same isolated vessel, and within the same lymphangion. It could be also attributed to the uncertainty in inflow and outflow pressure adjustment. Another potential source of this variation is the cannulation micro-pipette resistance. For this reason, the experiments on lymphatic vessels were carried out with the same set of resistance-matched micro-pipettes.

Fig 7: Temporal resolution with respect to axial pressure gradient. A positive (adverse) axial pressure gradient indicates that the outflow reservoir is raised higher than the inflow one and flow is driven by the active vessel contraction. At a negative (favorable) axial pressure gradient flow occurs without the need of vessel contraction.

Figure 7 again shows the benefit of employing frame-straddling to measure the instantaneous velocity inside lymphangions. The median Δt is 10 ms for $\Delta P_{axial} = -3 cm H_2O$. Without frame-straddling a camera at working at 100 fps would have been necessary. At this ΔP_{axial} this is not very restrictive, but with frame-straddling the velocity can be measured with much lower fps, resulting into less data to process for a certain measurement duration, or allowing PIV measurements for longer periods of time. At the other extreme, at high negative axial pressure gradients, 10k fps would be necessary without frame-straddling, resulting in a large number of pairs of frames and reducing the measurement duration due to camera memory limitations. Thus, the method employed

by Dixon and co-workers[9] would be challenged at high negative axial pressure gradients since even at zero gradient a camera with 1000-2000 fps capability is generally required. On the other hand, this is not a concern with the current method, as the temporal resolution is mainly limited by camera inter-frame time, which, for modern PIV cameras, is of the order of nanoseconds.

3.3 Lymphatic valves

Eddies around the leaflets of a thoracic duct valve were recorded with the μ-PIV system. Video S1 (Fig. 8a) of the accompanying multimedia material shows such an eddy, recorded with CW illumination at 1000 fps. The translumenal pressure was set at $2\ cmH_2O$ and the flow was driven by an axial pressure gradient of $-1\ cmH_2O$. These eddies were first reported by Florey in 1927 in guinea-pig lymphatic vessels.[46] Eddies around valve leaflets were also observed in mesenteric lymphatic vessels. Video S2 (Fig. 8b) and video S3 (Fig. 8c) show recirculation at negative ($-0.5\ cmH_2O$) and positive ($+0.5\ cmH_2O$) pressure gradient, respectively, at $2\ cmH_2O$ translumenal pressure, recorded at 500 fps in PM illumination.

(a)

(b)

Fig 8: Videos around valve leaflets: (a) Thoracic duct valve at negative pressure gradient (MP4, 16.7 MB), (b) Mesenteric valve at negative pressure gradient (MP4, 6.2 MB) and (c) Mesenteric valve at positive pressure gradient (MP4, 5.7 MB)

(c)

Fig 8: Videos around valve leaflets: (a) Thoracic duct valve at negative pressure gradient (MP4, 16.7 MB), (b) Mesenteric valve at negative pressure gradient (MP4, 6.2 MB) and (c) Mesenteric valve at positive pressure gradient (MP4, 5.7 MB)

The PIV system was also able to resolve quantitatively secondary flows in the regions behind valve leaflets (Fig. 9). The spatial resolution of PIV provides means of visualizing and quantifying these flow structures with much greater detail than other flow diagnostic techniques. On closer inspection of Figure 9b, however, the velocity inside the valve appears to be zero; clearly this cannot be the case. Arguably, this result may be due to geometrical asymmetries in the valve region and out-of-plane particle motion. The microscope optics were focused so that the image plane coincided with the mid-plane of the straight vessel segment close to the valve; the plane of maximum velocity between the valve leaflets may not necessarily coincide with the latter. Out-of-plane particle motion and noise from the valve leaflets may also be additional factors affecting the measurement in this region.

(a) (b)

Fig 9: Eddies forming around valve leaflets at an axial pressure gradient of $-1 cmH_2O$ at a translumenal pressure of 1 cmH_2O. This measurement was performed in a non contracting vessel and therefore the flow was at steady state. Approximately 100 pair of frames were acquired and the results averaged. Only one third of the velocity vectors are plotted for clarity. (a) Streamlines identifying recirculation around the lymphatic valve. (b) Colormap of the velocity magnitude. The scale is in mm/s. The Reynolds number calculated upstream the valve is approximately 0.45

3.4 Lymphatic vessels

The system developed was also able to measure the transient flow rate throughout the contraction cycle over a wide range of hydrodynamic conditions. The image processing time was approximately $1\ s$ for the vessel wall detection and $2\ s$ for the cross-correlation per pair of frame on a laptop with an Intel Core 2 Duo T9500 CPU.

The results of a flow measurement in a lymphatic vessel containing 3 valves and pumping against an adverse pressure gradient[‖] are shown in Figure 10 in solid lines; the dash-dot line depicts the vessel diameter. In this case five contractions cycle occur in 20 seconds, thus the contraction frequency is approximately 15 beats per minute. Flow rate, calculated by integrating the velocity profile at a cross section using the trapezoidal rule and assuming that the vessel has a circular cross section, is shown in Figure 10(a). Most of the positive flow (area under the solid curve) appears to take place during vessel distension and not contraction. This observation demonstrates that flow in any lymphangion depends on what is going on in the upstream and downstream lymphangions. Our preliminary results suggest that this is not a general case, but occurs frequently. The maximum velocity and WSS are shown in Figures 10(b) and 10(c), respectively.

When a favorable axial pressure gradient is imposed, positive flow occurs during when the vessel is distended, whereas lymphatic contraction reduces the flow rate, owing to the increase in vessel resistance as a result of vessel diameter reduction. Video S2 is of a lymphatic valve at favorable pressure gradient $-0.5\ cmH_2O$. As the vessel contracts flow stops. This video also demonstrates that with appropriate cannulation of the vessel it is possible to keep the particles at the mid-plane of the lymphangion in focus; occasionally a vessel may move so that the particles go out of focus and it is necessary to attempt a re-cannulation.

[‖]The output reservoir is higher than the input one

Another example is shown in Figure 11 which shows the flow rate and diameter tracings at the middle of a straight segment of a lymphatic vessel with 3 valves, during imposed favorable pressure gradient of $-1.0\ cmH_2O$. In addition, it is interesting that a sudden drop in flow rate is observed, but the vessel remains at its EDD at the flow rate drop time. This indicates an increase in flow resistance somewhere along the vessel that may be attributed to an out-of-phase contraction of an upstream or downstream lymphangion that is outside the FOV of the experiment. Again, as in the results shown in Figure 10, the sudden drop in flow rate demonstrates that the flow in a lymphangion may be affected by the contraction state of upstream and downstream lymphangions.

(a)

(b)

Fig 10:
Temporal variation of flow parameters and vessel diameter at adverse axial pressure gradient (a): Flow rate (solid line) and vessel diameter (dash-dot line), (b): Maximum velocity (solid line) and diameter (dash-dot line) (cont'd)

(c)

Fig 10: Temporal variation of flow parameters and vessel diameter at adverse axial pressure gradient (c): PIV derived WSS (solid line) and diameter (dash-dot line)

Fig 11: Temporal variation of Flow rate (solid line) and vessel diameter (dash-dot line) at favorable axial pressure gradient

4 Discussion

LEDs offer a versatile, low cost, safer alternative source of illumination to lasers for microfluidic flow measurements. The use of LED micro-PIV systems in physiological flow studies is relatively novel, and their potential has yet to be fully realized. The previous study by Willert et al.[47] showed that the driving current can be increased dramatically, without damaging the LEDs. Although the driving electronics limited the maximum current to 36A, the development of custom electronics that can pulse the LEDs with currents in the range of 200A, will enable the use of even shorter duration pulses and allow the measurements of even faster flows.

The apparatus and results of the present study are promising, and demonstrate, for the first time, the feasibility of the micro-PIV technique to quantify the two-dimensional flow field within contracting lymphatic vessels. The system described in this report represents a significant improvement in terms of spatial and temporal resolution compared to previous work. At 20x magnification, the system is capable of measuring velocities in excess of 100 mm/s (lower at higher magnification).[44] It may seem counter-intuitive that lymphatic flow velocity can reach such values, however we have observed velocities in the range of 50 mm/s at high negative axial pressure gradient (results not shown). Even for slower velocities the present implementation with frame straddling requires less memory for image storage and allows longer image acquisition times with the same available camera memory.

The likelihood of thermal damage is also reduced with respect to a laser based system. In fact, our results indicate that the likelihood of significant damage to the vessel caused by the LED is minimal. In our preparations the vessels attained a physiologic rate of contraction of 7.4 contractions per minute**. The measurements were performed for no more than 60 seconds at a time in

**Mean value 7.4 min^{-1}, standard deviation 2.9 min^{-1}, n = 11 vessels

any case, owing to camera memory limitations, with short duration light pulses; a considerable amount of light is also lost in the optical system or absorbed from the water bath. We were able to keep the vessels functioning for up to 4 hours, which corresponds to other experiments with continuous-wave illumination.

As an in vitro method, it allows measurements under a controlled environment; flow can be measured under varied hydrodynamic conditions as well as under constant ones with the additional chemical or electrical stimuli. This is expected to create new insight into lymphatic flow.

It may also be feasible to extend the method to *in vivo* flow measurements, provided there is optical access to the vessels. More work will be necessary to that end however, as an appropriate route of particle administration needs to be established. In addition, LEDs are also a cold light source, which may prevent dehydration or thermally-induced damage to the vessels. The lower photo-toxicity of pulsed LED illumination compared to conventional light sources (e.g., mercury, halogen) is why the latter sources are being superseded.[48] Thus μ-PIV has the potential to become a valuable tool for studying the lymphatic system and may also provide experimental validation of computational models that have recently appeared in the literature.[49,50]

The system proved able to reveal flow patterns around valves, which was previously only feasible with computational fluid dynamics tools.[49] However, this is a more challenging measurement than flow in straight segments. Flow around and inside valves is of interest, as it has been shown that the endothelial cells produce Nitric Oxide (NO), a substance that affects smooth muscle cell contractility. It is likely that there is a shear dependent mechanism that influences NO production, which varies locally in lymphatic vessels.[49,51] In order to quantify the complex flow patterns present around valves, the apparatus may be extended to allow 3D characterization of the flow field. Several different approaches to 3D μ-PIV exist, such as stereoscopic, holographic and aber-

ration based imaging. For a review of 3D implementations the reader is referred to the review by Cierpka and Kaehler.[44]

One drawback of the current setup, in fact of all μ-PIV equipment, is the restricted field of view of the available microscope objectives. The magnification of the objective employed in this study represents the optimal magnification for flow measurement based on the vessel average diameter of approximately 100 μm. Unfortunately, the resulting FOV at 20x magnification does now allow for simultaneous imaging of adjacent upstream/downstream lymphangions, which may be contracting out of phase with respect to the lymphangion under observation. Reducing the magnification will of course increase the FOV but at the expense of spatial resolution. Larger diameter particles may be needed in such circumstances which may give rise to issues depending on their settling velocity. Although the phase relationships of contraction between adjacent lymphangions and the effect on the flow cannot be studied with the current implementation, the use of micro-electromechanical deformable mirrors may offer a solution to this problem.[52] Customized confocal microscope designs with wider FOV have have recently appeared in the literature, which may offer a potential solution to this problem.[53]

The present implementation of WSS estimation assumes that the normal to the vessel wall is orthogonal to the main flow direction. This is not always the case with lymphatic vessels due to the contraction and the fact that the vessel wall may not be straight. An improved approach would need to determine the normal vector at the wall location were WSS are to be computed and derive the velocity gradient with respect to this normal direction. This approach was used by Poelma and co-workers,[54] but was not implemented here and is left as future work.

5 Conclusions

The preliminary data presented in this manuscript demonstrate the practical application of μ-PIV in measuring the flow field inside contracting lymphatic vessels with greater spatial and temporal resolution than has been achieved to date, and at far lower cost than equivalent laser-based systems.

The current system does have some limitations in terms of its hardware and software implementation. The hardware implementation limits the FOV and the 2-dimensional nature of the measurement limits the applicability of the measurement in the valve region, however, we are confident that these limitations may be overcome with appropriate improvements to hardware and software.

The present study has extended the applicability of μ-PIV to lymphatic flow measurements *in vitro*. As an *in-vitro* method has an advantage over *in-situ* or *in-vivo* methods in the fact that external stimuli such as pressure or chemical environment may be accurately controlled and their effect of flow may be derived. In contrast, the obvious disadvantage lies in the fact that it is not possible to measure flow in *in-vivo* conditions at present. Further work is needed in finding a route of particle administration at sufficient concentration, potentially in a lymph node. If successful the method has the potential to permit measurement *in situ*. Accurate measurement of the flow field in these vessels will provide insight into their function by way of providing the means of quantifying the fluidic environment and correlating its effect with changes in contractile behavior.

Acknowledgments

The authors are grateful to the Royal Society of Edinburgh for the award of a John Moyes Lessels travel scholarship to KM for his visit to Texas A&M University; also the University of Strathclyde for providing the PhD studentship awarded to KM and funding the development of the micro-PIV system. KM is also indebted to Dr J. Moore, Jr. and Dr D. Zawieja for hosting his visit in their labs and Dr Moore's PhD student Mohammad Jafarnejad for his help during his first visit to Texas A&M.

JM gratefully acknowledges the support of the USA National Institutes of Health, grants R01 HL 094269 and U01HL123420, the UK Royal Academy of Engineering and a UK Royal Society-Wolfson Research Merit Award.

DZ and ZN gratefully acknowledge grant NIH HL09655 by the USA National Institutes of Health.

During the development phase of the light source, a Nikon microscope and two Photron camera (as part of a micro-PIV system) were supplied on loan from the UK Engineering & Physical Sciences Research Council instrument pool. KM wishes to thank Dr Keith Matthieson and Dr Nial McAllinden from the Institute of Photonics, University of Strathclyde, UK for providing laboratory space for the micro-PIV system on loan, as well as for giving access to the power meter and spectrometer.

KM acknowledges the input of Dr Paul Murray (Department of Electronic & Electrical Engineering, Strathclyde University, UK) in image edge detection algorithms and Dr. Christos Diou (Department of Electrical and Computer Engineering, Aristotle University of Thessaloniki, Greece) for developing the algorithm used in this manuscript in Matlab.

References

1 M. A. Swartz, "The physiology of the lymphatic system," *Advanced Drug Delivery Reviews* **50**(1-2), 3–20 (2001).

2 K. N. Margaris and R. A. Black, "Modelling the lymphatic system: challenges and opportunities," *Journal of the Royal Society Interface* **9**, 601–612 (2012).

3 M. Muthuchamy, A. Gashev, N. Boswell, N. Dawson, and D. Zawieja, "Molecular and functional analyses of the contractile apparatus in lymphatic muscle," *Faseb Journal* **17**, 920+ (2003).

4 A. Galbis and A. Maestre, *Vector Analysis Versus Vector Calculus*, Springer (2010).

5 J. B. Dixon, D. C. Zawieja, A. A. Gashev, and G. L. Cote, "Measuring microlymphatic flow using fast video microscopy," *Journal of Biomedical Optics* **10**(6), 7 (2005).

6 J. B. Dixon, S. T. Greiner, A. A. Gashev, G. L. Cote, J. E. Moore, and D. C. Zawieja, "Lymph flow, shear stress, and lymphocyte velocity in rat mesenteric prenodal lymphatics," *Microcirculation* **13**(7), 597–610 (2006).

7 J. B. Dixon, *A biomedical engineering approach to investigating flow and wall shear stress in contracting lymphatics*. PhD thesis, Biomedical Engineering Department, Texas A&M University (2006).

8 T. Kassis, A. B. Kohan, M. J. Weiler, M. E. Nipper, R. Cornelius, P. Tso, and J. Brandon Dixon, "Dual-channel in-situ optical imaging system for quantifying lipid uptake and lymphatic pump function," *Journal of Biomedical Optics* **17**(8), 086005–086005 (2012).

9 J. B. Dixon, A. A. Gashev, D. C. Zawieja, J. E. Moore, and G. L. Cote, "Image correlation

algorithm for measuring lymphocyte velocity and diameter changes in contracting microlymphatics," *Annals of Biomedical Engineering* **35**(3), 387–396 (2007).

10 M. Onizuka, T. Flatebo, and G. Nicolaysen, "Lymph flow pattern in the intact thoracic duct in sheep," *Journal of Physiology-London* **503**(1), 223–234 (1997).

11 T. Naito, Y. Ozawa, M. Tomoyasu, M. Inagaki, M. Fukue, M. Sakai, T. Yamamoto, S. Ishikawa, and M. Onizuka, "New method for evaluation of lung lymph flow rate with intact lymphatics in anaesthetized sheep," *Acta Physiologica* **188**(2), 139–149 (2006).

12 J. G. McGeown, N. G. McHale, I. C. Roddie, and K. Thornbury, "Peripheral lymphatic responses to outflow pressure in anesthetized sheep," *Journal Of Physiology-London* **383**, 527–536 (1987).

13 I. Fedosov, V. Tuchin, E. Galartzha, A. Solov'eva, and T. Stepanova, "Recording of lymph flow dynamics in microvessels using correlation properties of scattered coherent radiation," *Quantum Electronics* **32**, 970–974 (2002).

14 V. Kalchenko, Y. Kuznetsov, I. Meglinski, and A. Harmelin, "Label free in vivo laser speckle imaging of blood and lymph vessels," *Journal of Biomedical Optics* **17**(5), 050502–1–050502–3 (2012).

15 E. I. Galanzha, E. V. Shashkov, V. V. Tuchin, and V. P. Zharov, "In vivo multispectral, multiparameter, photoacoustic lymph flow cytometry with natural cell focusing, label-free detection and multicolor nanoparticle probes," *Cytometry Part A* **73A**(10), 884–894 (2008).

16 M. Swartz, D. Berk, and R. Jain, "Transport in lymphatic capillaries .1. Macroscopic measurements using residence time distribution theory," *American Journal of Physiology-Heart and Circulatory Physiology* **270**, H324–H329 (1996).

17 D. Berk, M. Swartz, A. Leu, and R. Jain, "Transport in lymphatic capillaries .2. Microscopic velocity measurement with fluorescence photobleaching," *American Journal of Physiology-Heart and Circulatory Physiology* **270**, H330–H337 (1996).

18 M. Fischer, U. K. Franzeck, I. Herrig, U. Costanzo, S. Wen, M. Schiesser, U. Hoffmann, and A. Bollinger, "Flow velocity of single lymphatic capillaries in human skin," *American Journal of Physiology - Heart and Circulatory Physiology* **270**(1), H358–H363 (1996).

19 R. J. Adrian and J. Westerweel, *Particle Image Velocimetry*, Cambridge University Press (2011).

20 R. Sharma, W. Wang, J. C. Rasmussen, A. Joshi, J. P. Houston, K. E. Adams, A. Cameron, S. Ke, S. Kwon, M. E. Mawad, and E. M. Sevick-Muraca, "Quantitative imaging of lymph function," *American Journal of Physiology-Heart and Circulatory Physiology* **292**(6), H3109–H3118 (2007).

21 S. Kwon and E. M. Sevick-Muraca, "Noninvasive quantitative imaging of lymph function in mice," *Lymphatic Research and Biology* **5**(4), 219–231 (2007).

22 Z. Zhi, Y. Jung, and R. K. Wang, "Label-free 3D imaging of microstructure, blood, and lymphatic vessels within tissue beds in vivo," *Optics Letters* **37**, 812–814 (2012).

23 S. Yousefi, Z. Zhi, and R. Wang, "Label-free optical imaging of lymphatic vessels within tissue beds in vivo," *Selected Topics in Quantum Electronics, IEEE Journal of* **20**, 15–24 (2014).

24 R. Lindken, M. Rossi, S. Grosse, and J. Westerweel, "Micro-particle image velocimetry (mu piv): Recent developments, applications, and guidelines," *Lab on a Chip* **9**(17), 2551–2567 (2009).

25 W. T. Lai, D. C. Bjorkquist, M. P. Abbott, and A. A. Naqwi, "Video systems for piv recording," *Measurement Science & Technology* **9**(3), 297–308 (1998).

26 M. Raffel, *Particle image velocimetry : a practical guide*, Springer Verlag (2007).

27 Polysciences Inc., *Microspheres & Particles Handling Guide*.

28 M. Olsen and R. Adrian, "Out-of-focus effects on particle image visibility and correlation in microscopic particle image velocimetry," *Experiments in Fluids* **29**, S166–S174 (2000). 3rd International Workshop on Particle Image Velocimetry, Santa Barbara, California, SEP 16-18, 1999.

29 M. Rossi, R. Segura, C. Cierpka, and C. J. Kaehler, "On the effect of particle image intensity and image preprocessing on the depth of correlation in micro-PIV," *Experiments in Fluids* **52**, 1063–1075 (2012).

30 S. T. Wereley and C. D. Meinhart, "Recent advances in micro-particle image velocimetry," *Annual Review of Fluid Mechanics* **42**, 557–576 (2010).

31 A. A. Gashev, M. J. Davis, M. D. Delp, and D. C. Zawieja, "Regional variations of contractile activity in isolated rat lymphatics," *Microcirculation* **11**(6), 477–492 (2004).

32 E. I. Galanzha, V. V. Tuchin, and V. P. Zharov, "Advances in small animal mesentery models for in vivo flow cytometry, dynamic microscopy, and drug screening," *World Journal of Gastroenterology* **13**, 192–218 (2007).

33 W. Thielicke and E. Stamhuis, "PIVlab - towards user-friendly, affordable and accurate digital particle image velocimetry in matlab," *Journal of Open Research Software* **2**(1) (2014).

34 L. Gui, S. Wereley, and S. Lee, "Digital filters for reducing background noise in micro-piv," in *11th Intl. Symposium on Appl. of Laser Techniques to Fluid Mechanics*, (2002).

35 M. Honkanen and H. Nobach, "Background extraction from double-frame PIV images," *Experiments in Fluids* **38**, 348–362 (2005).

36 N. G. Deen, P. Willems, M. v. S. Annaland, J. A. M. Kuipers, R. G. H. Lammertink, A. J. B. Kemperman, M. Wessling, and W. G. J. van der Meer, "On image pre-processing for PIV of single- and two-phase flows over reflecting objects," *Experiments in Fluids* **49**, 525–530 (2010).

37 C. V. Nguyen, A. Fouras, and J. Carberry, "Improvement of measurement accuracy in micro PIV by image overlapping," *Experiments in Fluids* **49**, 701–712 (2010).

38 D. Garcia, "A fast all-in-one method for automated post-processing of PIV data," *Experiments in Fluids* **50**, 1247–1259 (2011).

39 D. Garcia, "Robust smoothing of gridded data in one and higher dimensions with missing values," *Computational Statistics & Data Analysis* **54**(4), 1167 – 1178 (2010).

40 W. Burger and M. J. Burge, *Principles of Digital Image Processing*, Springer Verlag (2009).

41 E. C. Lee, H. C. Lee, and K. R. Park, "Finger Vein Recognition Using Minutia-Based Alignment and Local Binary Pattern-Based Feature Extraction," *International Journal of Imaging Systems and Technology* **19**(3), 179–186 (2009).

42 H. B. Kim, J. R. Hertzberg, C. Lanning, and R. Shandas, "In vitro study of wall shear stress measurement using a non invasive echo piv technique," in *Proceedings of the ASME Summer Bioengineering Conference*, 71–72 (2003).

43 J. Westerdale, M. Belohlavek, E. M. McMahon, P. Jiamsripong, J. J. Heys, and M. Milano, "Flow velocity vector fields by ultrasound particle imaging velocimetry," *Journal of Ultrasound Medicine* **30**(2), 187–195 (2011).

589 44 C. Cierpka and C. J. Kaehler, "Particle imaging techniques for volumetric three-component
590 (3D3C) velocity measurements in microfluidics," *Journal of Visualization* **15**, 1–31 (2012).
591 45 R. J. Adrian, "Dynamic ranges of velocity and spatial resolution of particle image velocime-
592 try," *Measurement Science and Technology* **8**(12), 1393 (1997).
593 46 H. Florey, "Observations on the contractility of lacteals: Part i," *The Journal of physiology*
594 **62**(3), 267–72 (1927).
595 47 C. Willert, B. Stasicki, J. Klinner, and S. Moessner, "Pulsed operation of high-power light
596 emitting diodes for imaging flow velocimetry," *Measurement Science & Technology* **21**(7),
597 11 (2010).
598 48 R. Cole, "Live-cell imaging," *Cell Adhesion & Migration* **8**(5), 452–459 (2014).
599 49 J. T. Wilson, W. Wang, A. H. Hellerstedt, D. C. Zawieja, and J. E. Moore, "Confocal image-
600 based computational modeling of nitric oxide transport in a rat mesenteric lymphatic vessel,"
601 *Journal of Biomechanical Engineering* **135**, 051005–1 (2013).
602 50 J. T. Wilson, R. van Loon, W. Wang, D. C. Zawieja, and J. E. M. Jr., "Determining the
603 combined effect of the lymphatic valve leaflets and sinus on resistance to forward flow,"
604 *Journal of Biomechanics* , – (2015).
605 51 H. G. Bohlen, O. Y. Gasheva, and D. C. Zawieja, "Nitric oxide formation by lymphatic bulb
606 and valves is a major regulatory component of lymphatic pumping," *American Journal of*
607 *Physiology-Heart and Circulatory Physiology* **301**, H1897–H1906 (2011).
608 52 B. Potsaid and J. T.-Y. Wen, "Adaptive scanning optical microscope: large field of
609 view and high-resolution imaging using a MEMS deformable mirror," *Journal of Micro-*
610 *Nanolithography MEMS and MOEMS* **7**, 021009:1–10 (2008).

611 53 R. Webb and F. Rogomentich, "Confocal microscope with large field and working distance,"
612 *Applied Optics* **38**, 4870–4875 (1999).
613 54 C. Poelma, K. Van der Heiden, B. P. Hierck, R. E. Poelmann, and J. Westerweel, "Measure-
614 ments of the wall shear stress distribution in the outflow tract of an embryonic chicken heart,"
615 *Journal of the Royal Society Interface* **7**, 91–103 (2010).

Dr. Margaris received his MEng degree in Mechanical Engineering from the Aristotle University of Thessaloniki, Greece in 2003. After working in the industry as a mechanical engineer, he returned to higher education and obtained an MSC in Bioengineering and a Ph.D. in Biomedical Engineering from the University of Strathclyde, Glasgow, UK, in 2010 and 2015, respectively. Currently, he is working in an engineering consultancy for the offshore energy industries.

Dr. Nepiyushchikh is a Research Scientist at the Mechanical Engineering Department of Georgia Institute of Technology. Dr. Nepiyushchikh received her M.D. from State Medical Academy, St. Petersburg, Russia in 1996. Prior to her current appointment, she was a Postdoctoral Associate at Texas A&M Health Science Center doing research on molecular mechanism of contractility lymphatic vessels under the direction of Prof. David Zawieja. She explores how mechanical forces, immune and cancer cells affect pumping activity of lymphatic vessels.

Dr. Zawieja is currently the Regents Professor and Interim Chair Medical Physiology and Director of the Lymphatic Biology Division at Texas A&M Health Science Center. He received his Ph.D. in Physiology from Medical College of Wisconsin in 1986. His primary research area is the function of the lymphatic system, the factors that regulate and modulate lymph transport and its relation with pathologies such as atherosclerosis, metabolic syndrome and diabetes.

Prof. Moore received his Ph.D. from the Georgia Institute of Technology, and postdoctoral training at the Swiss Institute of Technology at Lausanne. Prior to moving to Imperial College London in 2013, Prof. Moore worked at Texas A&M University, serving as the Carolyn S. and Tommie E. Lohman 59 Professor. He currently serves as the Bagrit and Royal Academy of Engineering Chair in Medical Device Design. His research interests include Biomechanics, Devices, and the

Lymphatic System.

Dr. Black is a biomedical engineer with over 25 years experience in the field and a long-standing interest in the fluid mechanics of the cardiovascular system in health and disease. He graduated BSc (Hons) Engineering Science from the University of Edinburgh, and gained his PhD at the University of Liverpool. A chartered scientist and engineer, he is a Fellow of the Institution of Mechanical Engineers and the Institute of Physics and Engineering in Medicine.

List of Figures

2 Example of frame straddling (F-S). The camera is set to record at a specific frame rate. In order to acquire one pair of images for PIV, the first light pulse is placed towards the end of the first frame (Frame 1A) and the second light pulse at the beginning of the second frame (Frame 1B) as to 'straddle' the inter-frame time. With this approach the time between frames is limited by the camera inter-frame time, or 2 μs in the current implementation. The next pair of frames (Frames 2A/2B) must be acquired at half the camera fps in order to avoid double exposure.

3 Image of a lymphatic vessel and valve at 20x magnification: (a) bright-field and (b) side-scattering illumination mode. Here, light was delivered from a fibre-optic cable positioned above and at an angle of about 45 degrees with respect to the microscope stage. The low numerical aperture of the objective used (M = 20x, NA = 0.5) ensured that stray light from the bottom wall was not significant.

4 Image processed by a combination of unsharp and smoothing filters prior to PIV analysis.

5 Example of vessel wall detection. The red line denotes the detected vessel wall edge using Canny edge detection.

6 Power output of two white LEDs by Luminus Devices, CBT-90 and CBT-140. The measurement was performed at the exit of a 6 ft fiber-optic light guide. Despite the considerable losses at the LED/fiber-optic bundle interface, the power output is sufficient for optical flow diagnostic methods, such as the one presented here.

7 Temporal resolution with respect to axial pressure gradient. A positive (adverse) axial pressure gradient indicates that the outflow reservoir is raised higher than the inflow one and flow is driven by the active vessel contraction. At a negative (favorable) axial pressure gradient flow occurs without the need of vessel contraction.

8 Videos around valve leaflets: (a) Thoracic duct valve at negative pressure gradient (MP4, 16.7 MB), (b) Mesenteric valve at negative pressure gradient (MP4, 6.2 MB) and (c) Mesenteric valve at positive pressure gradient (MP4, 5.7 MB)

9 Eddies forming around valve leaflets at an axial pressure gradient of $-1\ cmH_2O$ at a translumenal pressure of $1\ cmH_2O$. This measurement was performed in a non contracting vessel and therefore the flow was at steady state. Approximately 100 pair of frames were acquired and the results averaged. Only one third of the velocity vectors are plotted for clarity. (a) Streamlines identifying recirculation around the lymphatic valve. (b) Colormap of the velocity magnitude. The scale is in mm/s. The Reynolds number calculated upstream the valve is approximately 0.45

10 Temporal variation of flow parameters and vessel diameter at adverse axial pressure gradient (a): Flow rate (solid line) and vessel diameter (dash-dot line), (b): Maximum velocity (solid line) and diameter, (c): PIV derived WSS (solid line) and diameter (dash-dot line)

11 Temporal variation of Flow rate (solid line) and vessel diameter (dash-dot line) at favorable axial pressure gradient

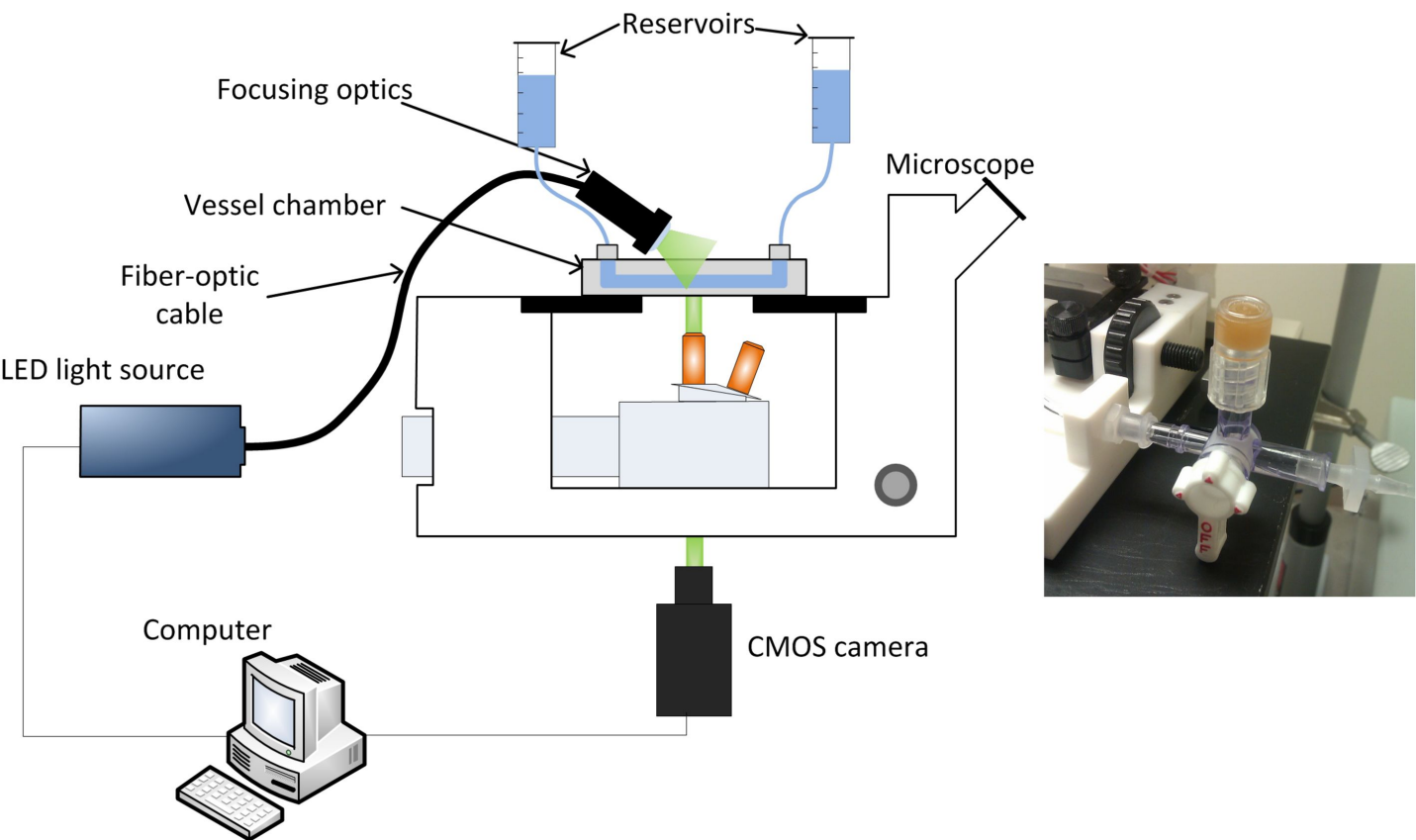
Reservoirs
Focusing optics
Microscope
Vessel chamber
Fiber-optic cable
LED light source
Computer
CMOS camera

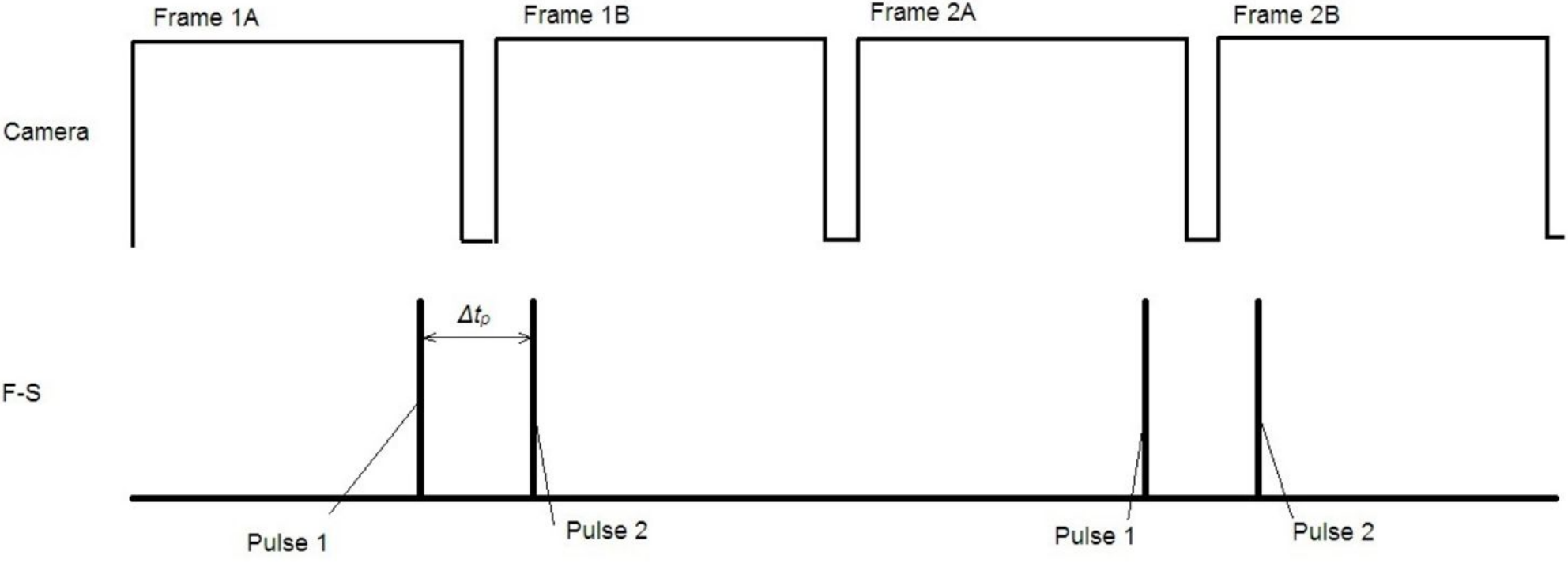
Frame 1A
Frame 1B
Frame 2A
Frame 2B
Camera
F-S
Δt_p
Pulse 1
Pulse 2
Pulse 1
Pulse 2

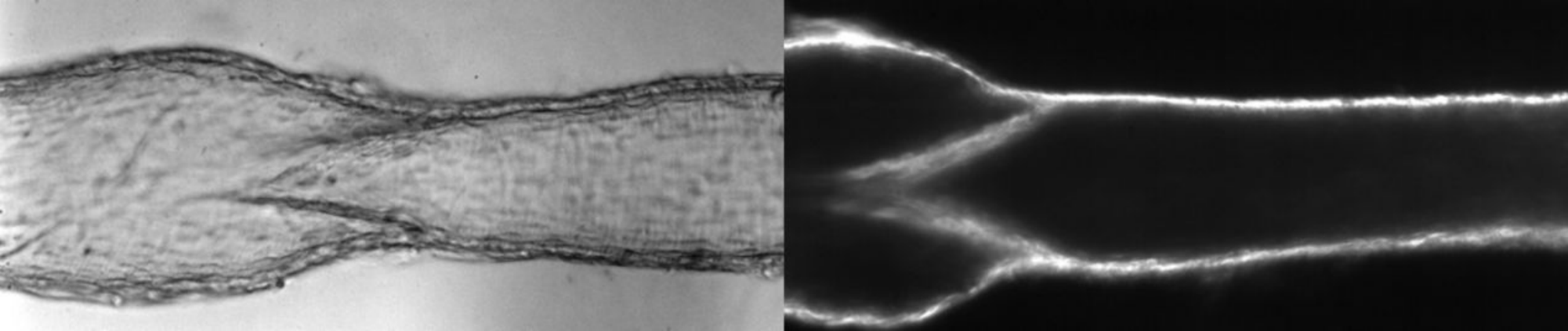

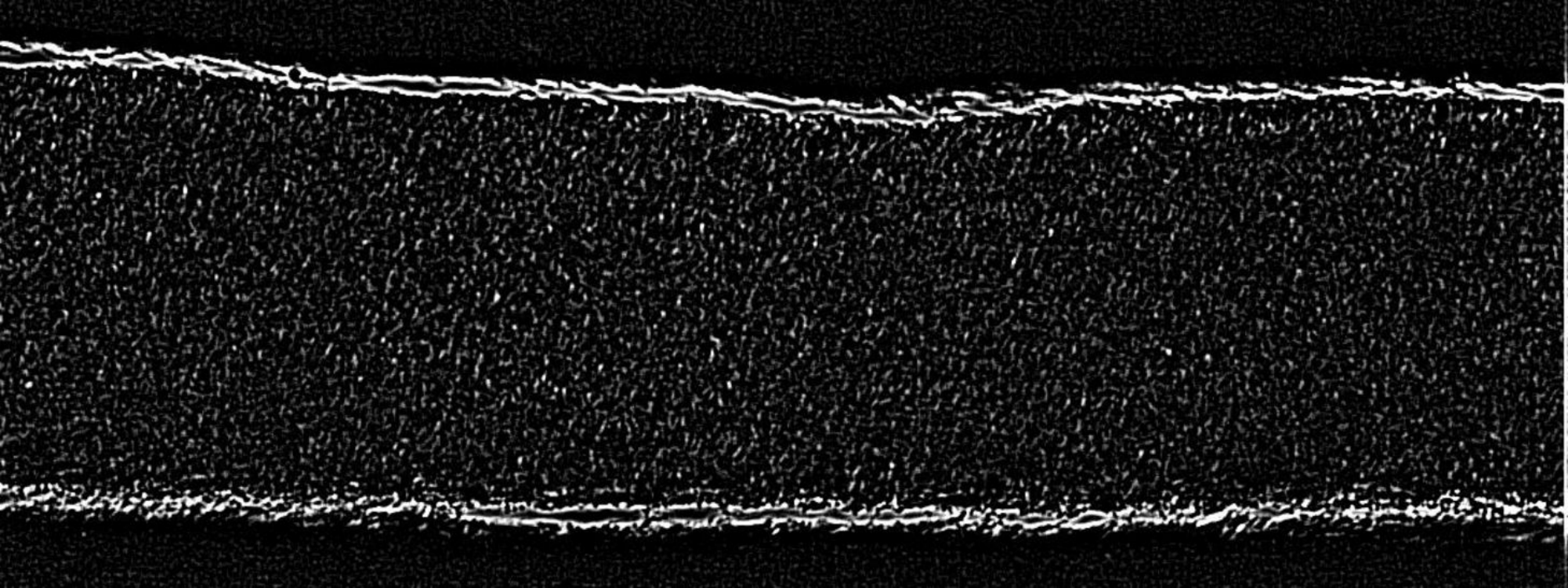

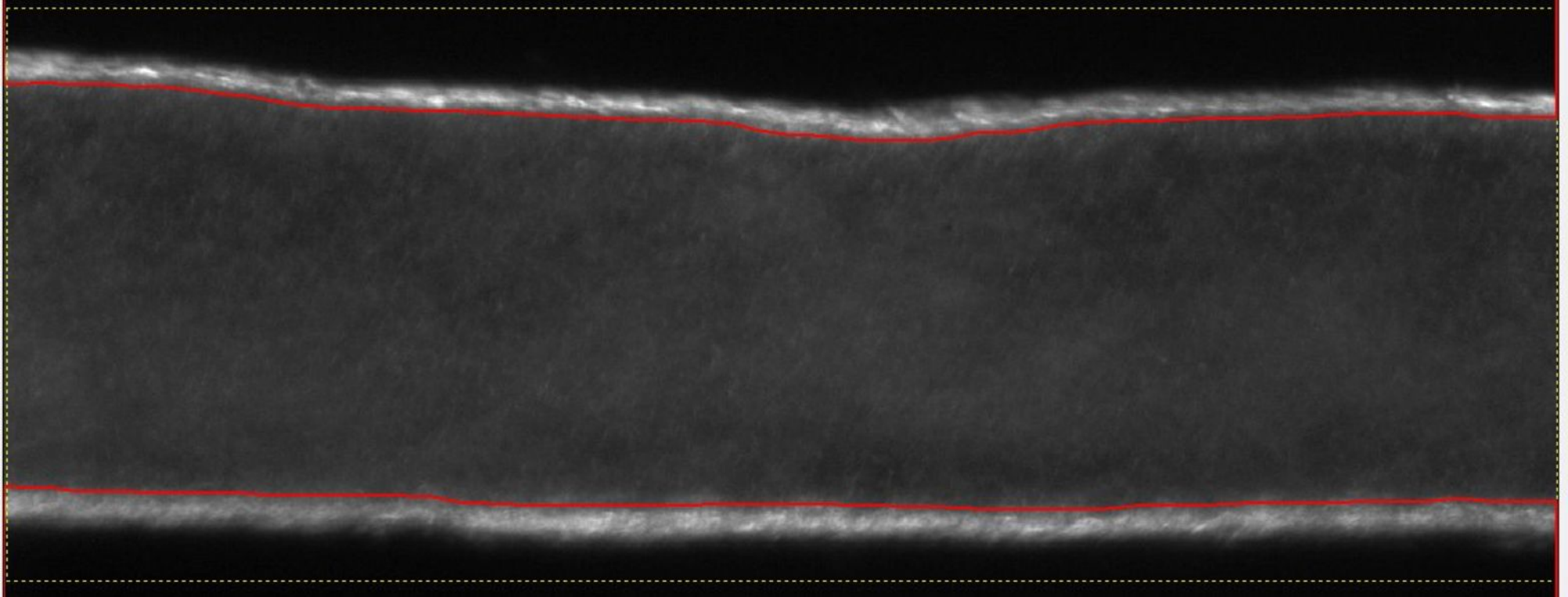

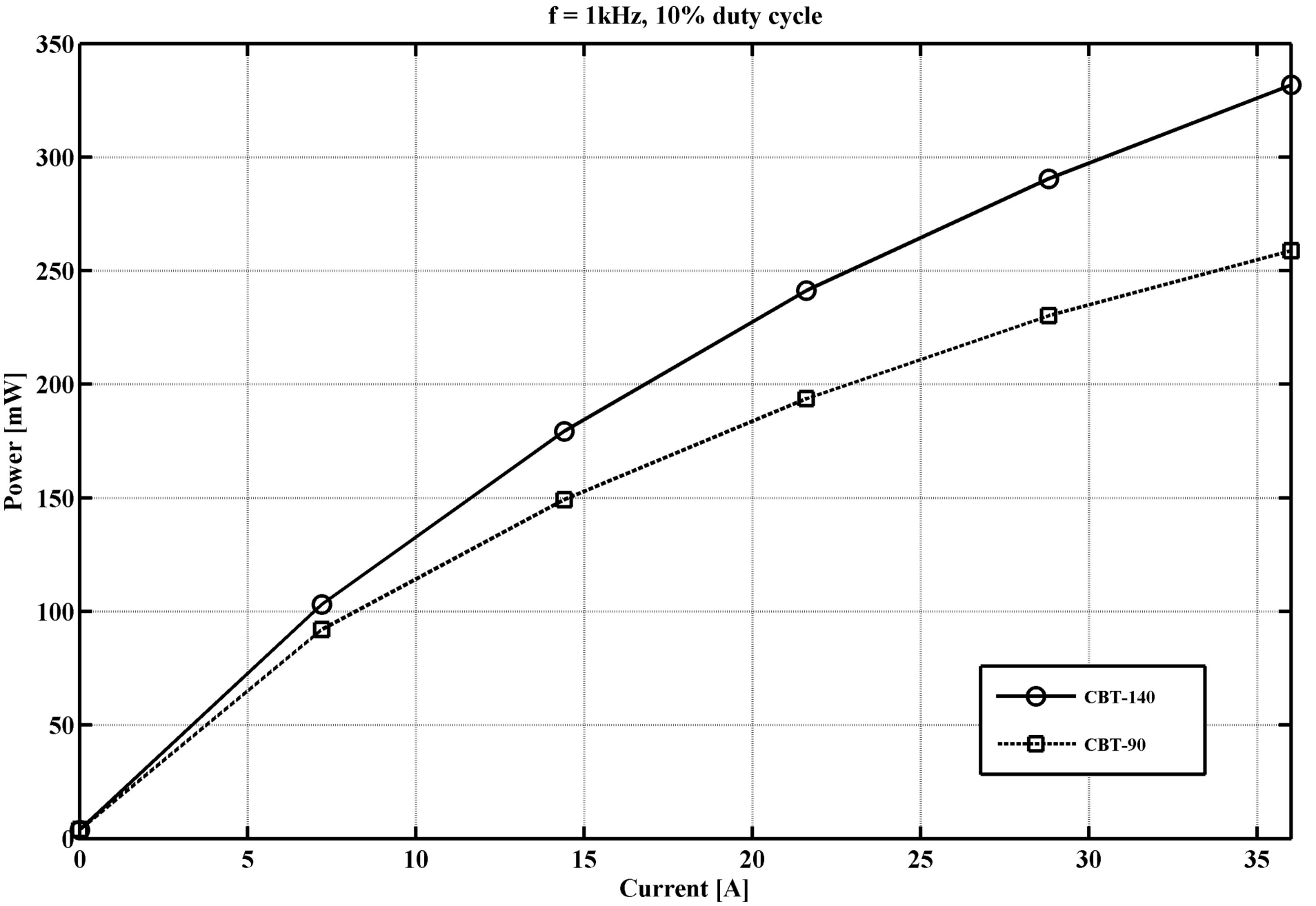
f = 1kHz, 10% duty cycle
Power [mW]
Current [A]
0
50
100
150
200
250
300
350
0
5
10
15
20
25
30
35
CBT-140
CBT-90

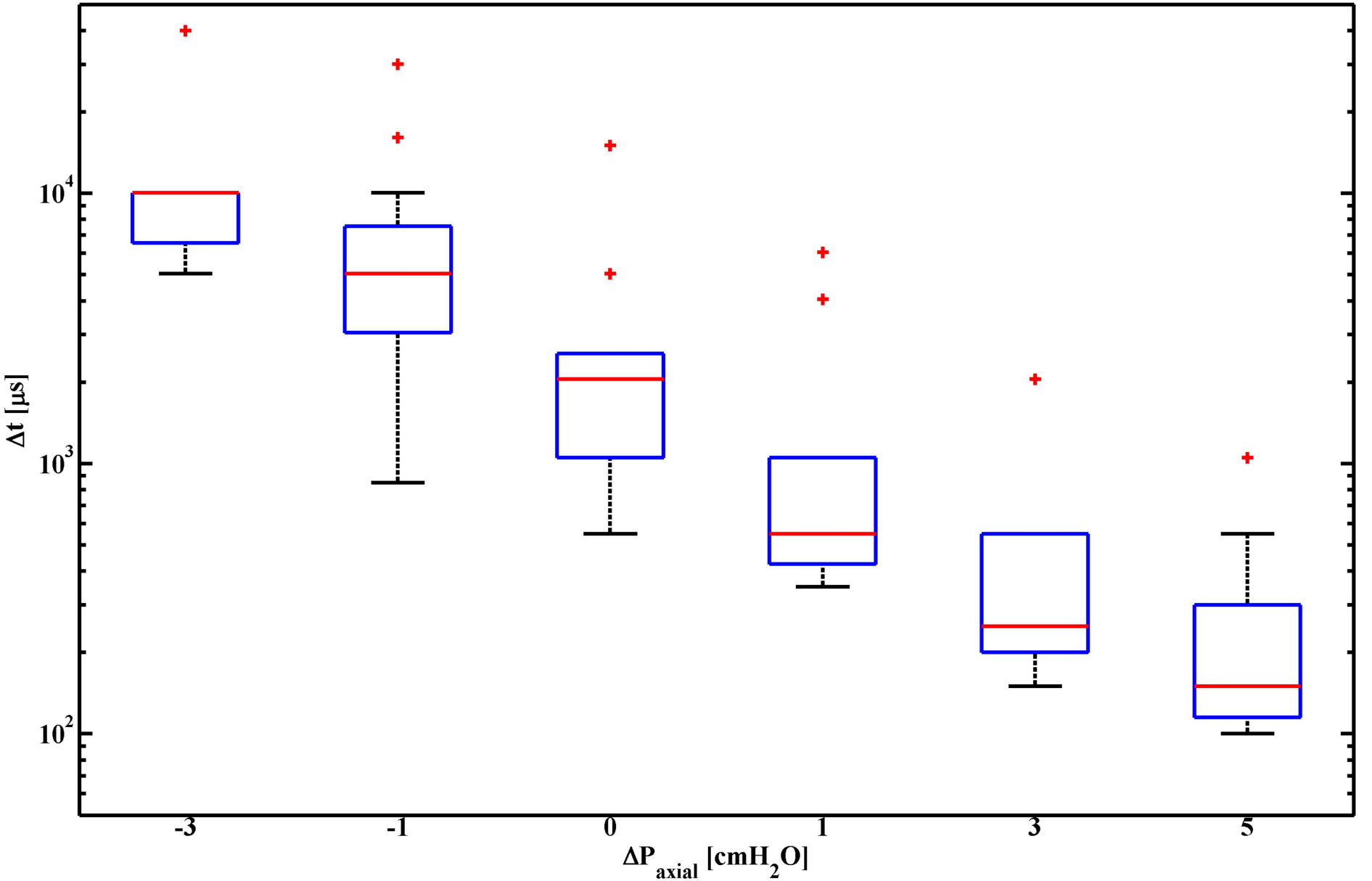
10^4
10^3
10^2
Δt [μs]
-3
-1
0
1
3
5
ΔP_{axial} [cmH_2O]

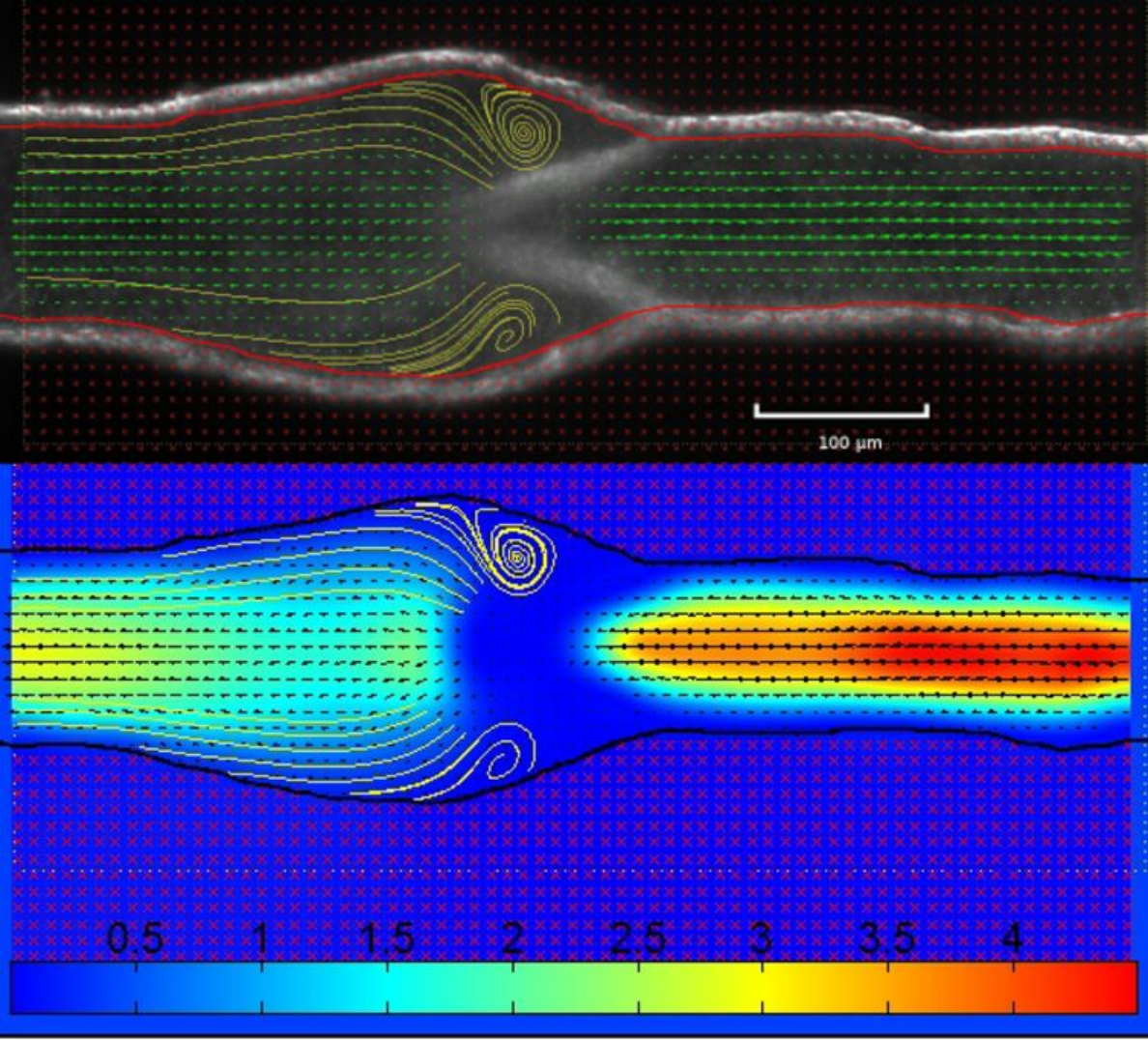
100 µm
0.5
1
1.5
2
2.5
3
3.5
4

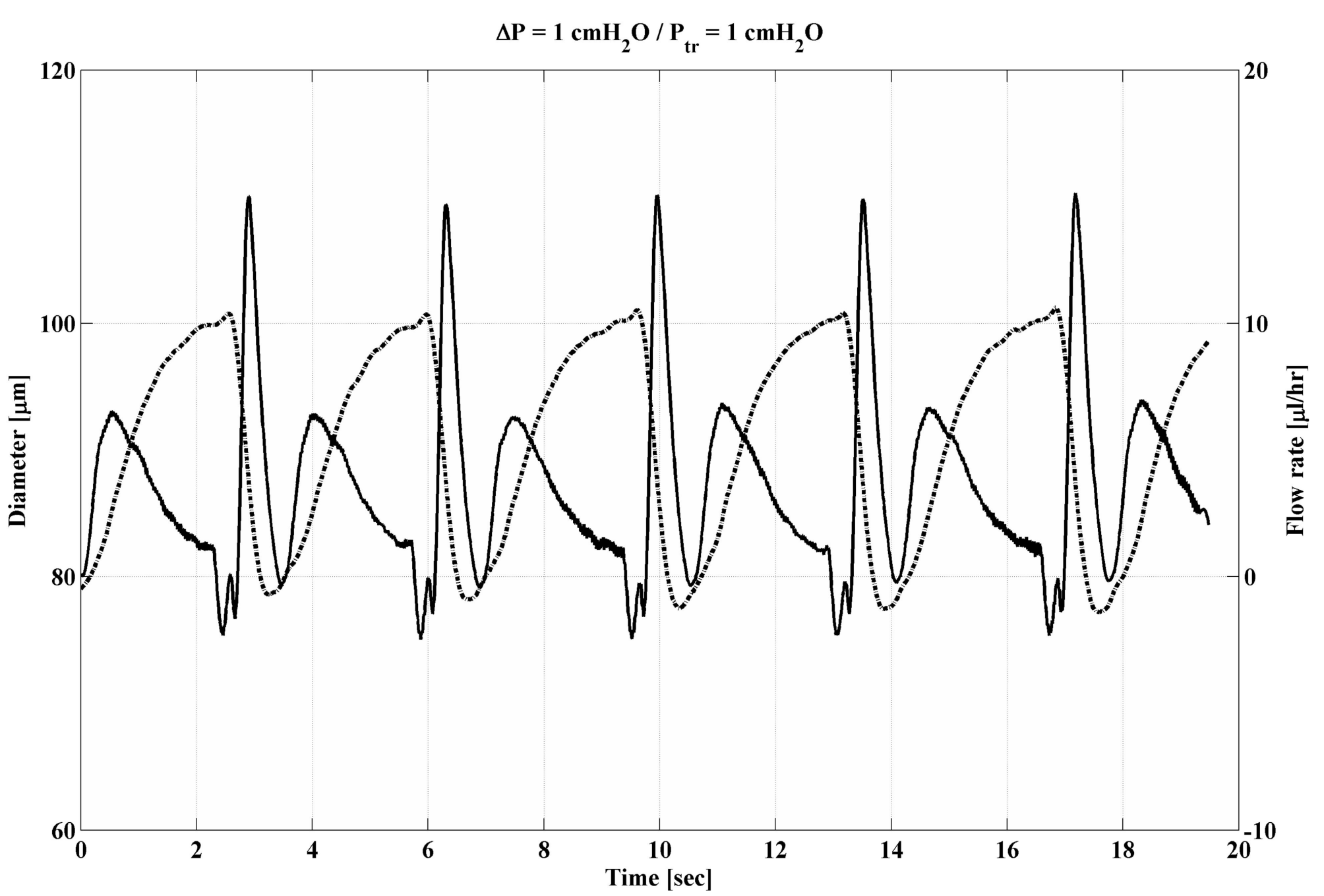
ΔP = 1 cmH2O / Ptr = 1 cmH2O
Diameter [μm]
Flow rate [μl/hr]
120
100
80
60
20
10
0
-10
0
2
4
6
8
10
12
14
16
18
20
Time [sec]

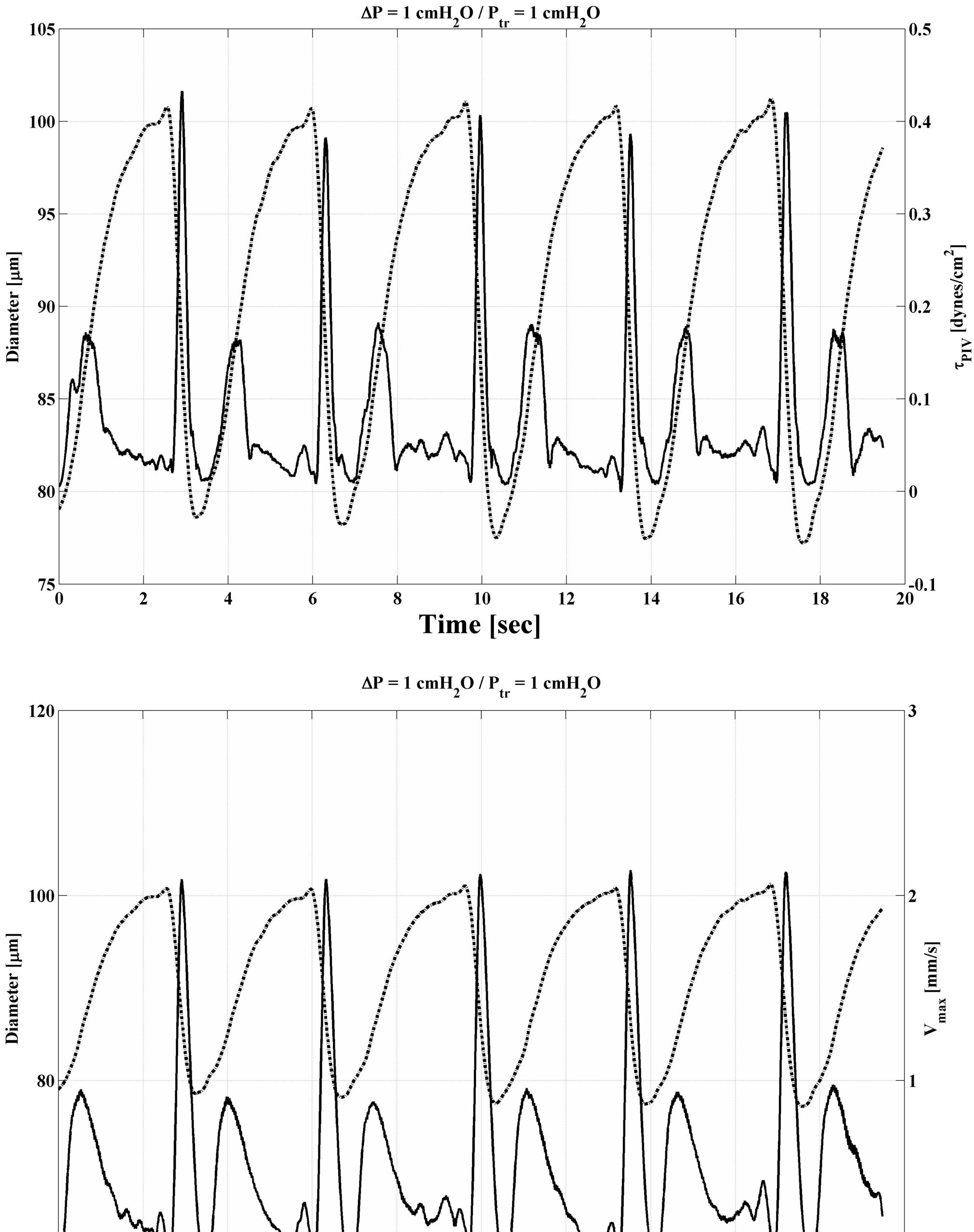
ΔP = 1 cmH2O / Ptr = 1 cmH2O
Diameter [μm]
τPIV [dynes/cm2]
105
100
95
90
85
80
75
0.5
0.4
0.3
0.2
0.1
0
-0.1
0
2
4
6
8
10
12
14
16
18
20
Time [sec]

ΔP = 1 cmH2O / Ptr = 1 cmH2O
Diameter [μm]
Vmax [mm/s]
120
100
80
60
3
2
1
0
0
2
4
6
8
10
12
14
16
18
20
Time [sec]

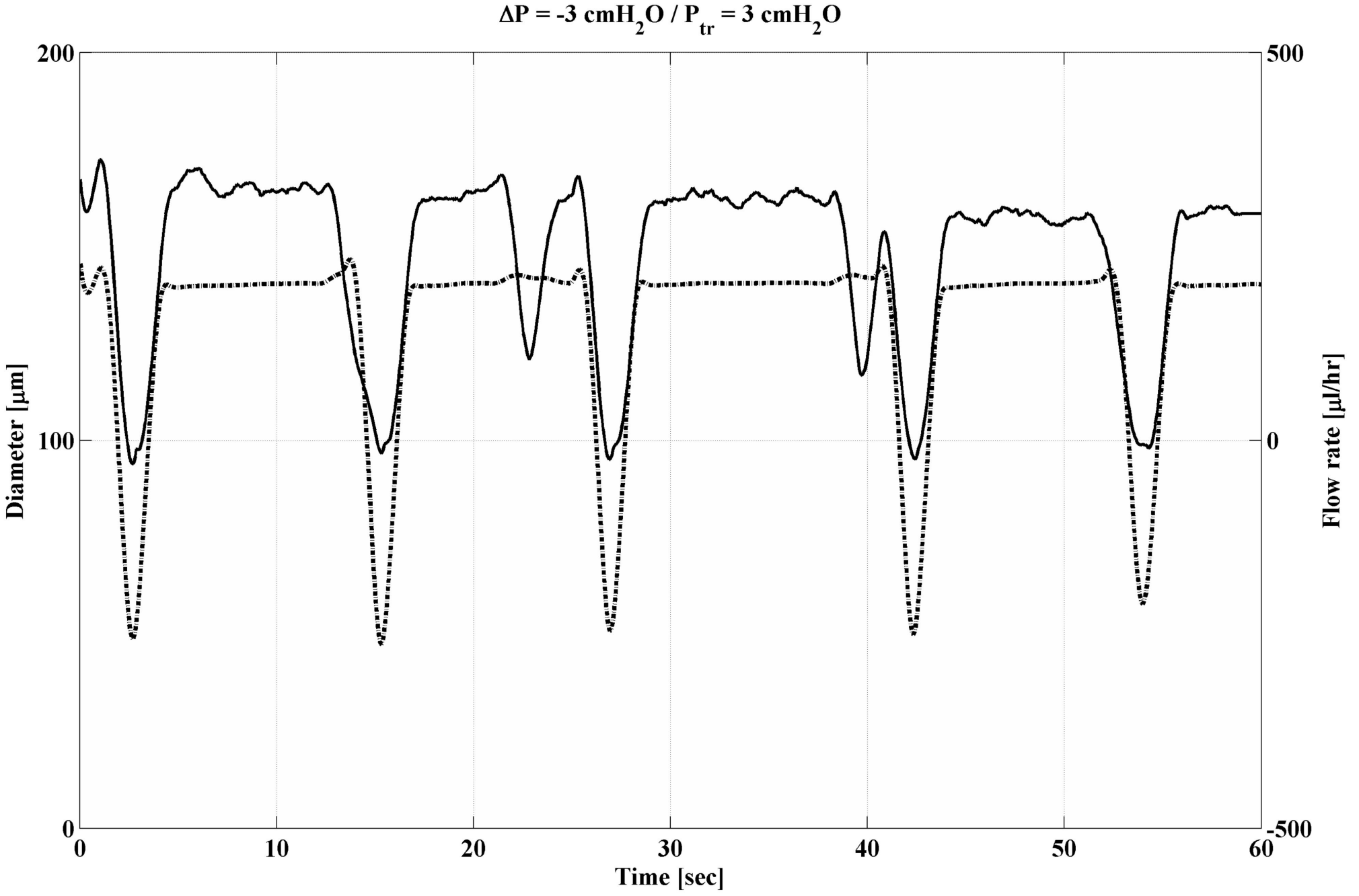
ΔP = -3 cmH2O / Ptr = 3 cmH2O
200
100
0
500
0
-500
Diameter [μm]
Flow rate [μl/hr]
0
10
20
30
40
50
60
Time [sec]